Inorganic Chemistry
Article

Inorg. Chem. **2010**, *49*, 10571–10578 **10571**
DOI: 10.1021/ic101529n

Site-Differentiated Solid Solution in $(Na_{1-x}Cu_x)_2Ta_4O_{11}$ and Its Electronic Structure and Optical Properties

Olena Palasyuk, Andriy Palasyuk, and Paul A. Maggard*

Department of Chemistry, North Carolina State University, Raleigh, North Carolina 27695-8204, United States

Received July 29, 2010

The $(Na_{1-x}Cu_x)_2Ta_4O_{11}$ ($0 \leq x \leq 0.78$) solid-solution was synthesized within evacuated fused-silica vessels and characterized by powder X-ray diffraction techniques (space group: $R\bar{3}c$ (#167), $Z = 6$, $a = 6.2061(2)-6.2131(2)$ Å, $c = 36.712(1)-36.861(1)$ Å, for $x = 0.37$, 0.57, and 0.78). The structure consists of single layers of TaO_7 pentagonal bipyramids as well as layers of isolated TaO_6 octahedra surrounded by Na^+ and Cu^+ cations. Full-profile Rietveld refinements revealed a site-differentiated substitution of Na^+ cations located in the 12*c* (Wyckoff) crystallographic site for Cu^+ cations in the 18*d* crystallographic site. This site differentiation is driven by the linear coordination geometry afforded at the Cu^+ site compared to the distorted seven-coordinate geometry of the Na^+ site. Compositions more Cu-rich than $x \sim 0.78$, that is, closer to "$Cu_2Ta_4O_{11}$", could not be synthesized owing to the destabilizing Na^+/Cu^+ vacancies that increase with x up to the highest attainable value of ~26%. The UV−vis diffuse reflectance spectra show a significant red-shift of the bandgap size from ~4.0 eV to ~2.65 eV with increasing Cu^+ content across the series. Electronic structure calculations using the TB-LMTO-ASA approach show that the reduction in bandgap size arises from the introduction of Cu $3d^{10}$ orbitals and the formation of a new higher-energy valence band. A direct bandgap transition emerges at $\vec{k} = \Gamma$ that is derived from the filled Cu $3d^{10}$ and the empty Ta $5d^0$ orbitals, including a small amount of mixing with the O 2p orbitals. The resulting conduction and valence band energies are determined to favorably bracket the redox potentials for water reduction and oxidation, meeting the thermodynamic requirement for photocatalytic water-splitting reactions.

Introduction

Many early transition-metal oxide photocatalysts have been investigated for their photon-driven heterogeneous catalysis of water into oxygen and/or hydrogen, such as known for La-doped $NaTaO_3$,[1,2] $La_2Ti_2O_7$,[3,4] and many others that exhibit photon-conversion efficiencies of ~15−50%.[5,6] However, owing to their large bandgap sizes, their use has so far been predominantly restricted to the ultraviolet energy range. The investigation of new metal oxides exhibiting visible-light bandgap sizes is therefore essential to facilitate the development of new technologies for the conversion of solar energy to chemical fuels. To address this need, current strategies for decreasing the bandgap sizes have focused on the creation of higher-energy valence bands via the incorporation of a late transition metal or main group element, that is, as found in $AgNbO_3$ or $PbTiO_3$.[7,8] In these systems, the higher-energy valence bands originate from the filled d^{10} or $d^{10}s^2$ electron configurations, and not predominantly from the O 2p orbitals as found in the larger bandgap metal oxides. Further, this type of band profile approach should attempt to maintain suitable energetic positions with respect to the redox couples for the oxidation and reduction half-reactions of water.

Our research efforts in this area have focused on the investigation of new heterometallic oxides and oxide/organic hybrid solids containing Cu(I) (d^{10}) in combination with an early transition metal, for example, Nb(V) (d^0). Recent results for hybrid oxide/organic solids demonstrate substantial reductions in bandgap sizes, down to ~2.0−2.6 eV, because of the formation of higher-energy valence bands derived from the Cu $3d^{10}$ orbitals.[9−11] However, the optical and photocatalytic properties of simpler heterometallic oxides, for example, as in the Cu(I)-tantalates, remain almost entirely unexplored. The $Cu_2O-Ta_2O_5$ system is character-

---

*To whom correspondence should be addressed. Phone: (+1) 919-515-3616. Fax: (+1) 919-515-5079. E-mail: paul_maggard@ncsu.edu.

[1] Kato, H.; Asakura, K.; Kudo, A. *J. Am. Chem. Soc.* **2003**, *125*, 3082–3089.

[2] Porob, D.; Maggard, P. A. *J. Solid State Chem.* **2006**, *179*, 1727–1732.

[3] Kim, H. G.; Hwang, D. W.; Bae, S. W.; Jung, J. H.; Lee, J. S. *Catal. Lett.* **2003**, *91*, 193–198.

[4] Arney, D.; Porter, B.; Greve, B.; Maggard, P. A. *J. Photochem. Photobiol., A* **2008**, *199*, 230–235.

[5] Osterloh, F. E. *Chem. Mater.* **2008**, *20*, 35–54.

[6] Kudo, A.; Miseki, Y. *Chem. Soc. Rev.* **2009**, *38*, 253–278.

[7] Kato, H.; Kobayashi, H.; Kudo, A. *J. Phys. Chem. B* **2002**, *106*, 12441–12447.

[8] Kim, H. G.; Becker, O. S.; Jang, J. S.; Ji, S. M.; Borse, P. H.; Lee, J. S. *J. Solid State Chem.* **2006**, *179*, 1214–1218.

[9] Lin, H.; Maggard, P. A. *Inorg. Chem.* **2006**, *46*, 1283–1290.

[10] Lin, H.; Maggard, P. A. *Inorg. Chem.* **2009**, *48*, 8940–8946.

[11] Lin, H.; Maggard, P. A. *Cryst. Growth Des.* **2010**, *10*, 1323–1331.

© 2010 American Chemical Society

Published on Web 10/11/2010

ized by a family of structurally-related solids with the general formula $Cu_xTa_{3n+1}O_{8n+3}$.[12,13] Their structures are composed of different stacking variants of both single ($n = 1$) and/or double layers ($n = 2$) of edge-shared TaO_7 pentagonal bipyramids, where the n in the formula is the average number of single and double layers in the structure. These pentagonal bipyramidal layers alternate with layers of linearly-coordinated Cu(I) and isolated TaO_6 octahedra. Interestingly, a full occupancy of the Cu site is only achieved for $n = 2$, that is, for $Cu_3Ta_7O_{19}$. Owing to charge-balancing requirements, the other structures show increasing Cu-site vacancies with decreasing n, that is, from $n = 1.5$ for $Cu_5Ta_{11}O_{30}$ (16.6% vacant), to $n = 1.33$ for $Cu_7Ta_{15}O_{41}$ (22.3%), and for $n = 1$ in $Cu_2Ta_4O_{11}$ (33%). Only the two highest n members, $Cu_3Ta_7O_{19}$ and $Cu_5Ta_{11}O_{30}$, have been synthesized in pure form and characterized by X-ray diffraction (XRD) techniques.[14,15] The other structures have so far only been found as impurity phases in HREM studies.[12] Thus, major questions remain regarding their range of compositional stability, and which currently appears to decrease with n.

Presented herein is an investigation of the synthesis and characterization of the lowest n (= 1) composition in the "$M_2Ta_4O_{11}$" structure as part of the $(Na_{1-x}Cu_x)_2Ta_4O_{11}$ solid-solution. While $Na_2Ta_4O_{11}$ ($x = 0$) has been previously synthesized in pure form and characterized by single-crystal XRD,[16] the proposed "$Cu_2Ta_4O_{11}$" ($x = 1$) has only been reported as a possible impurity phase and has never been thoroughly characterized.[12] The new high-purity synthesis of the $(Na_{1-x}Cu_x)_2Ta_4O_{11}$ solid-solution allows a complete structural characterization for compositions approaching "$Cu_2Ta_4O_{11}$", and also provides a convenient probe to investigate the structural factors governing its stability or lack thereof. Notably, the $Na_2Ta_4O_{11}$ solid has also recently been reported as exhibiting high photocatalytic activity for hydrogen production when irradiated by ultraviolet light in aqueous solutions.[17] Thus, the slow and systematically controlled substitution of Cu^+ for Na^+ within its structure has been utilized to more closely track the creation and energy of the new higher-energy valence band, and which illustrates a novel route for its visible-light sensitization. Further, by using the band positions known for $Na_2Ta_4O_{11}$, the members of the $(Na_{1-x}Cu_x)_2Ta_4O_{11}$ solid-solution can be investigated for their conduction and valence band energies with respect to the redox potentials for water reduction and oxidation.

Experimental Section

Synthesis. Members of the $(Na_{1-x}Cu_x)_2Ta_4O_{11}$ ($0 \le x \le 0.78$) solid-solution were synthesized by combining stoichiometric amounts of Na_2O (Alfa Aesar, >99.9%), Cu_2O (Alfa Aesar, >99.9%), and Ta_2O_5 (Alfa Aesar, >99.99%) loaded at the Na:Cu:Ta molar ratios appropriate for $x = 0$, 0.1, 0.3, 0.5, 0.7, 0.9, and 1.0. The reactants were ground together inside a glovebox, flame-sealed inside of evacuated fused-silica tubes, and heated to 950 °C for ~5 days before subsequently being allowed to radiatively cool to room temperature. Thin platelet-shaped powders were obtained with colors that ranged from light white to deep yellow with increasing copper content. A powder X-ray diffraction (PXRD) analysis indicated good agreement with the theoretical pattern calculated using the $Na_2Ta_4O_{11}$ structural model, and no detectable impurity peaks for the reactions loaded at $x = 0$, 0.1, 0.3, 0.5, 0.7 (i.e., 0% to 70% Cu). Attempts to grow large single crystals suitable for single-crystal diffraction using a CuCl flux were unsuccessful. Reactions loaded at the Cu-richest ratios of $x = 0.9$ and 1.0 (i.e., 90% to 100% Cu) exhibited additional X-ray diffraction peaks characteristic of $Cu_5Ta_{11}O_{30}$, $Cu_3Ta_7O_{19}$, as well as some unidentified peaks. For our synthetic conditions, the Cu-rich limit of the solid solution was found to be $x \sim 0.78$ as shown by the regular changes in lattice constants that reach a plateau at this composition, and which was consistent with the limiting composition of the full-profile Rietveld refinement (below).

Structural Characterization. Three members of the solid solution $(Na_{1-x}Cu_x)_2Ta_4O_{11}$, that is, $x = 0.3$, 0.5, and 0.7 were selected for collection of high-resolution PXRD data at room temperature on a RIGAKU D/Max 2200 Powder X-ray diffractometer using Cu $K\alpha$ radiation. Diffraction data were collected in the 2θ range from 5° to 115° in step sizes of 0.02° and a dwell time of 4 s per step. Refinements were performed by the full-profile Rietveld method using the program FullProf.[18] The unit-cell dimensions and starting atomic positions were taken from the reported single-crystal structure of $Na_2Ta_4O_{11}$,[16] as well as from the HREM structural model proposed by Jahnberg for the "$Cu_2Ta_4O_{11}$" composition.[12] The tantalum-oxide substructure for both models is nearly identical. However, while the Na atoms fully occupy the 12*c* crystallographic site, the Cu atoms are located on the 18*d* site and are 2/3 occupied, as would be required for charge balancing. Two refinement approaches were investigated to refine the crystal structure of each of the $(Na_{1-x}Cu_x)_2Ta_4O_{11}$ solid-solution members. In the first approach, the Cu/Na atoms were allowed to refine as disordered on either the 12*c* or the 18*d* crystallographic sites. These refinements typically converged at $R_B \sim 0.08-0.14$ with unsatisfactory differential diffractograms. In the second approach, the Cu and Na atoms were allowed to refine in the 12*c* and 18*d* positions, respectively, with the restraint that the final occupancies yield the charge-balanced composition. This second model exhibited significantly better fits and reduction of the R_B/R_{wp} residuals to ~3−5%. The final refinements included 21 parameters (5,495 data points) and converged at $R_B = 5.3\%$ for $x = 0.3$, $R_B = 6.7\%$ for $x = 0.5$, and $R_B = 10.8\%$ for $x = 0.7$. In a typical refinement, initially only the zero-point shift and scale factor were refined. The lattice constants were then allowed to refine, followed by the background parameters that involved gradually increasing the polynomial used in the fit up to the sixth order. The positional parameters were refined next, beginning with the copper and tantalum atoms and followed by all oxygen atoms. This was followed by refinement of the isotropic thermal parameters for all atoms, and which were thereafter fixed to refine the occupancies. Afterward, profile-shape parameters were included with a peak-asymmetry correction for $2\theta < 40°$. Powder refinement parameters and interatomic distances are given in Tables 1 and 2, and the resulting fits of the Rietveld refinements to the experimental powder data are plotted in Figure 1.

Optical Measurements. The UV−Vis diffuse reflectance spectra were collected on a Shimadzu Spectrometer UV-3600/3100 with the use of an integrating sphere. Approximately 50 mg of each sample was mixed with barium sulfate and pressed onto a holder and placed along the external window of the integrating sphere. A second sample of pure pressed barium sulfate powder was prepared as a reference, and the data were plotted as the

---

(12) Jahnberg, L.; Sundberg, M. *J. Solid State Chem.* **1992**, *100*, 212–219.

(13) Jahnberg, L. *Acta Chem. Scand.* **1987**, *A41*, 527–532.

(14) Jahnberg, L. *J. Solid State Chem.* **1982**, *41*, 286–292.

(15) Palasyuk, O.; Palasyuk, A.; Maggard, P. A. *J. Solid State Chem.* **2010**, *183*, 814–822.

(16) (a) Mattes, R.; Schaper, J. *Rev. Chim. Miner.* **1985**, *22*(6), 817–820. (b) Ercit, T. S.; Hawthorne, F. C.; Cerny, P. *Bull. Miner.* **1985**, *108*, 541–549.

(17) Ratnamala, A.; Suresh, G.; Kumari, V. D.; Subrahmanyam, M. *Mater. Chem. Phys.* **2008**, *110*, 176–179.

(18) Rodriges-Carvajal, J. *FullProf*; Laboratoire Leon Brillouin, CEA-CNRS: Saclay, France, 1998.

Table 1. Crystal and Refinement Data for $(Na_{1-x}Cu_x)_2Ta_4O_{11}$ for x = 0.37, 0.57, and 0.78

	$(Na_{0.63(1)}Cu_{0.37})_2Ta_4O_{11}$	$(Na_{0.43(1)}Cu_{0.57})_2Ta_4O_{11}$	$(Na_{0.22(3)}Cu_{0.78})_2Ta_4O_{11}$
space group, Z	$R\bar{3}c$ (167), 6	$R\bar{3}c$ (167), 6	$R\bar{3}c$ (167), 6
unit cell			
a (Å)	6.2061(2)	6.2101(2)	6.2131(2)
c (Å)	36.712(1)	36.827(1)	36.861(1)
V (Å^3)	1224.5(3)	1229.9(3)	1232.3(3)
radiation	Cu K$_\alpha$ = 1.54056 Å	Cu K$_\alpha$ = 1.54056 Å	Cu K$_\alpha$ = 1.54056 Å
2θ range	5.0−115.0°	5.0−115.0°	5.0−115.0°
no. of data collected	5,494 data points	5,494 data points	5,495 data points
no. of unique data	216 Bragg reflections	217 Bragg reflections	219 Bragg reflections
no. of variables	21	21	21
residuals[a]	R_B = 0.067	R_B = 0.053,	R_B = 0.108

[a] $R_B = \sum|I_0 - I_c|/\sum I_0$.

Table 2. Atomic Coordinates, Equivalent Isotropic Displacement Parameters (Å^2), and Site Occupancies for $(Na_{0.63(1)}Cu_{0.37})_2Ta_4O_{11}$, $(Na_{0.43(1)}Cu_{0.57})_2Ta_4O_{11}$, and $(Na_{0.22(3)}Cu_{0.78})_2Ta_4O_{11}$

atom	Wyckoff position	symmetry	x	y	z	[a]U(eq)	Occ.≠ 1
Ta1	6*b*	−3.	0	0	0	0.70	
Ta2	18*e*	.2	0.3633(2) 0.3629(2) 0.3630(3)	0	1/4	0.30	
Na	12*c*	3.	0	0	0.169(1) 0.171(1) 0.169(1)	1.20	0.63(1) 0.43(1) 0.22(3)
Cu	18*d*	−1	1/2	0	0	1.20	0.24(1) 0.38(1) 0.52(3)
O1	18*e*	.2	3/4	0	1/4	1.70	
O2	12*c*	3.	0	0	0.0959(5) 0.0975(6) 0.0925(8)	1.70	
O3	36*f*	1	0.947(2) 0.951(2) 0.954(2)	0.361(2) 0.364(2) 0.373(3)	0.3042(4) 0.3055(3) 0.3065(4)	1.70	

[a] The equivalent isotropic displacement parameters were fixed during the final refinement.

remission function $F(R_\infty) = (1 - R_\infty)^2/(2R_\infty)$, where R is diffuse reflectance based on the Kubelka−Monk theory of diffuse reflectance.[19]

Electronic Structure Calculations. Electronic structure calculations were performed for the limiting compositions $Na_2Ta_4O_{11}$ and the idealized "$Cu_2Ta_4O_{11}$" using the linear muffin-tin orbital (LMTO) method in the atomic sphere approximation (ASA), within the tight-binding program TB-LMTO-ASA.[20] The radii of the Wigner−Seitz (WS) spheres were assigned automatically so that the overlapping potentials would be the best possible approximations to the full potentials, with the default 16% overlap restriction.[21] Since the title structures are rather open, special care was taken in filling the interatomic space. The use of only atom-centered spheres resulted in errors because the overlap was too large. Therefore, the empty interstitial spheres (ES) were added to the crystal potential and the basis set. The sphere radii and their positions were chosen so that space filling was achieved without exceeding a sphere overlap of 16%. All sphere positions and radii were calculated automatically; the WS radii (Å) were Na, 1.88 and Cu, 1.30; Ta, 1.33−1.41 and 1.35−1.37; O, 0.93−1.01 and 0.94−0.99; ES, 0.61−0.84 and 0.66−0.98 for $Na_2Ta_4O_{11}$ and $Cu_2Ta_4O_{11}$, respectively. The calculations used a basis set of Na 3s/3p orbitals, Cu 4s/4p/3d orbitals, Ta 6s/6p/5d orbitals, and O 2s/2p orbitals, and the reciprocal space integrations were performed on 12 × 12 × 12 grids of irreducible k-points using the tetrahedron method.[22] Semiempirical extended Hückel calculations were performed using the program package CAESAR,[23] with the following parameters (double-ζ-functions): H_{ij} (eV), ζ_1, coefficient 1, ζ_2, coefficient 2: Na: 3s −5.10, 0.733, 1.00, 0, 0; 3p −3.10, 0.733, 1.00, 0, 0; Cu: 4s −11.40, 2.20, 1.00, 0, 0; 4p −6.06, 2.20, 1.00, 0, 0; 3d −14.00, 5.95, 0.5933, 2.300, 0.5744; Ta: 6s −10.10, 2.28, 1.00, 0, 0; 6p −6.86, 2.241, 1.00, 0, 0; 5d −12.10, 4.762, 0.6815, 1.938, 0.5589; O: 2s −32.29999, 2.2775, 1.00, 0, 0, 2p −14.80, 2.275, 1.00, 0, 0.

Results and Discussion

Synthesis. Early systematic investigations of the $Cu_2O{-}Ta_2O_5$ system by Jahnberg revealed the existence of several possible layered copper(I)-tantalate solids belonging to a family having the general formula $A_xTa_{3n+1}O_{8n+3}$,[12−14] including $Cu_2Ta_4O_{11}$, $Cu_3Ta_7O_{19}$, $Cu_5Ta_{11}O_{30}$, and $Cu_7Ta_{15}O_{41}$. In these studies, only $Cu_5Ta_{11}O_{30}$ could be synthesized in pure form and characterized by means of single-crystal XRD. All other phases were obtainable only as side-products, and structural models were proposed based upon high-resolution electron microscopy (HREM) measurements. Synthetic difficulties in their preparation were attributed to their meta-stability

---

(19) Kortüm, G. *Reflectance Spectroscopy*, Springer-Verlag: New York, NY, 1996.

(20) Tank, R.; Jepsen, O.; Burkhardt, A.; Andersen, O. K. *TB-LMTO-ASA Program*, Version 4.7; Max-Plank-Institut für Festkörperforschung: Stutgart, Germany, 1995.

(21) Jepsen, O.; Andersen, O. K. *Z. Phys. B* **1995**, *97*(1), 35–47.

(22) Blöchl, P. E.; Jepsen, O.; Andersen, O. K. *Phys. Rev. B.* **1994**, *49*(23), 16223–16233.

(23) Ren, J.; Liang, W.; Whangbo, M.-H. *CAESAR*; PrimeColor Software Inc.: Raleigh, NC, U.S.A., 1998.

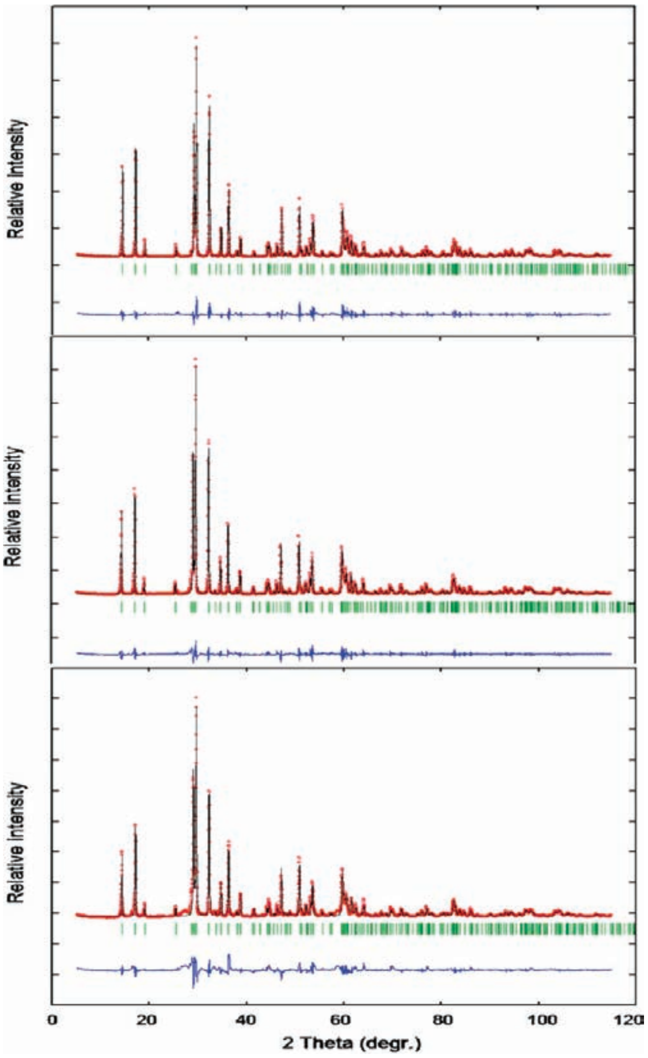

Figure 1. PXRD and Rietveld refinement results for $(Na_{0.63(1)}Cu_{0.37})_2Ta_4O_{11}$ (upper), $(Na_{0.43(1)}Cu_{0.57})_2Ta_4O_{11}$ (middle), and $(Na_{0.22(3)}Cu_{0.78})_2Ta_4O_{11}$ (lower). The observed profile is indicated by circles and the calculated profile by the solid line. Bragg peak positions are indicated by vertical tics, and the difference diffractogram is shown at the bottom.

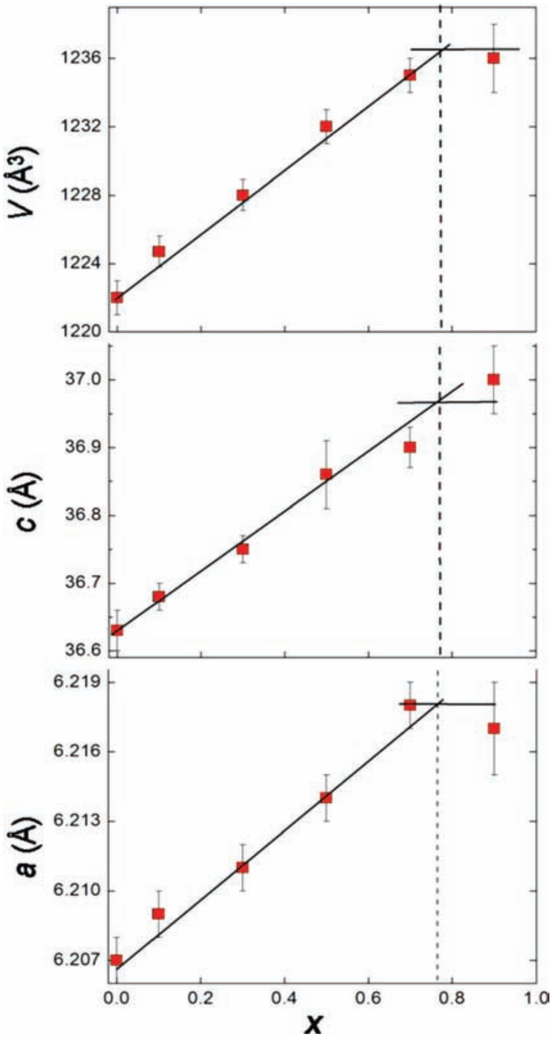

Figure 2. Plot of the unit-cell lattice parameters a (Å), c (Å), and V (Å^3), versus x across the $(Na_{1-x}Cu_x)_2Ta_4O_{11}$ solid solution.

Table 3. Selected Interatomic Distances in (**1**) $(Na_{0.63(1)}Cu_{0.37})_2Ta_4O_{11}$, (**2**) $(Na_{0.43(1)}Cu_{0.57})_2Ta_4O_{11}$, and (**3**) $(Na_{0.22(3)}Cu_{0.78})_2Ta_4O_{11}$

	distance		
bond	(**1**)	(**2**)	(**3**)
Ta1, Octahedron			
Ta1−O3 × 6	1.975(2)	1.967(3)	1.946(4)
Ta2, Pentagonal Bipyramid			
Ta2−O1 × 2	1.998(3)	1.998(3)	1.999(2)
Ta2−O1	2.400(3)	2.404(3)	2.405(6)
Ta2−O2 × 2	2.035(5)	2.052(5)	2.014(5)
Ta2−O3 × 2	2.066(4)	2.067(4)	2.073(5)
Na, Distorted Seven-Coordinate			
Na−O2	2.684(5)	2.707(5)	2.820(6)
Na−O3 × 3	2.477(4)	2.472(4)	2.396(5)
Na−O3 × 3	2.614(6)	2.577(4)	2.633(5)
Cu, Linear			
Cu−O3 × 2	1.807(4)	1.771(3)	1.764(4)

that arose from the high Cu(I) vacancies within the layers, which increases in the order of $Cu_3Ta_7O_{19}$ (0% site vacancies), $Cu_5Ta_{11}O_{30}$ (~17% site vacancies), $Cu_7Ta_{15}O_{41}$ (~22% site vacancies), and $Cu_2Ta_4O_{11}$ (~33% site vacancies), as well as to their compositional closeness owing to the inter-related stacking variants. In recent work we found that the synthesis of $Cu_3Ta_7O_{19}$ in pure form could be obtained via the use of a CuCl flux,[15] and enabling its first complete structural characterization by powder X-ray data refinements. Unfortunately, similar solid-state and flux synthetic approaches have so far not yielded either of the proposed $Cu_2Ta_4O_{11}$ or $Cu_7Ta_{15}O_{41}$ structures. Instead, solid-state reactions of Cu_2O and Ta_2O_5 loaded at molar ratios close to 2:4 or 7:15 were found to produce only $Cu_5Ta_{11}O_{30}$ and Cu_2O. Given that the analogous $Na_2Ta_4O_{11}$ is known, the partial substitution of Na_2O for Cu_2O in the reactants was systematically investigated as a possible means to stabilize the $Cu_2Ta_4O_{11}$ structure, and that yielded the high-purity preparation of the solid solution $(Na_{1-x}Cu_x)_2Ta_4O_{11}$. A plot of the refined lattice constants, shown in Figure 2, exhibits a linear Vegard's-law behavior over a compositional range extending between approximately $0 < x < 0.78$. Thus, the Cu-richest composition that could be

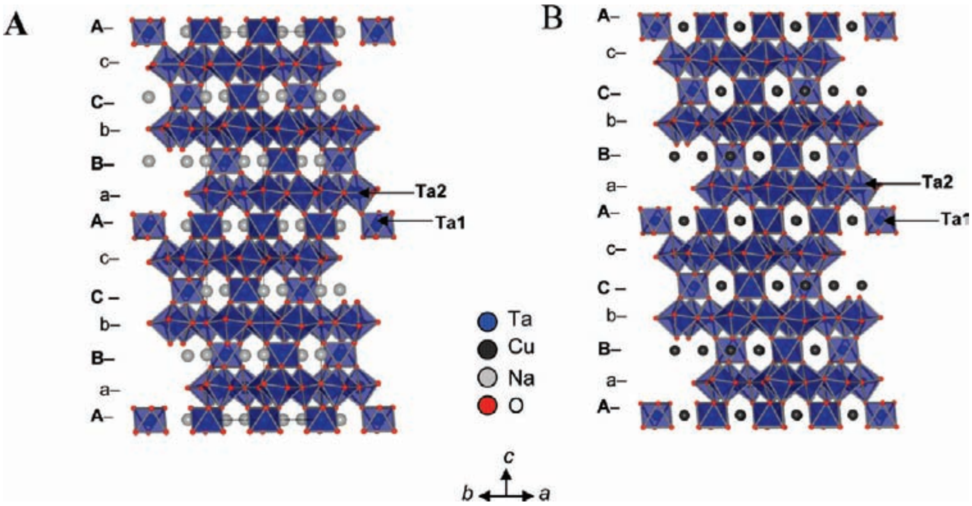

Figure 3. Polyhedral views down [110] for (a) $Na_2Ta_4O_{11}$ and (b) the proposed "$Cu_2Ta_4O_{11}$" structural model; blue polyhedra are TaO_7 pentagonal bipyramids and TaO_6 octahedra.

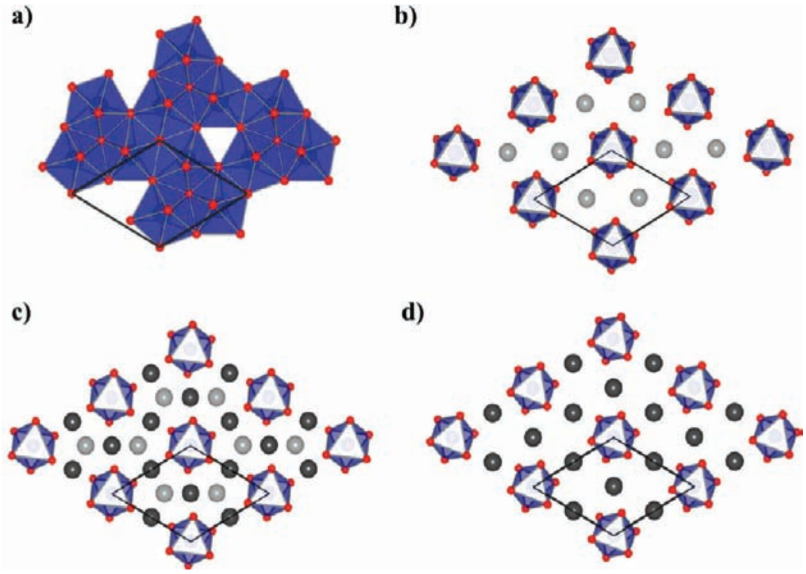

Figure 4. Structural views for $(Na_{1-x}Cu_x)_2Ta_4O_{11}$ down [001] of (a) a single layer of TaO_7 pentagonal bipyramids (blue polyhedra), and also the layer of TaO_6 octahedra and monovalent cations for (b) only Na (gray atoms), (c) both Na and Cu (black atoms), and (c) only Cu. The blue polyhedra in (b−d) are TaO_6 octahedra and all red atoms are oxygen.

formed using these synthetic procedures was $Na_{0.44}Cu_{1.56}Ta_4O_{11}$, and which exhibits a Cu-site position close to that proposed for the $Cu_2Ta_4O_{11}$ structural model (described below).

Structures. Three members of the $(Na_{1-x}Cu_x)_2Ta_4O_{11}$ ($0 \le x \le 0.78$) solid solution were structurally characterized with increasing Cu content with the compositions $x = 0.37$, 0.57 and 0.78, and thus falling between the $Na_2Ta_4O_{11}$ and proposed "$Cu_2Ta_4O_{11}$" compositions. Near-neighbor interatomic distances for each are listed in Table 3, and a plot of the refined lattice constants across the entire composition range is shown in Figure 2. Each structure contains layers of edge-shared TaO_7 pentagonal bipyramids that alternate with layers of isolated TaO_6 octahedra, as shown in Figure 3 and labeled as A/B/C or a/b/c, respectively. The TaO_6 octahedral coordination environment is formed by the apical O atoms of three edge-shared pentagonal bipyramids both above and below the layer, shown in Figure 5. The three apical O atoms are tilted toward each other and form a regular octahedral coordination environment with six equivalent Ta1−O3 distances of ~1.95−1.88 Å for all three structures. The TaO_7 pentagonal bipyramids are also fairly similar in all three structures, shown in Figure 4a, and are composed of six nearly equidistant Ta2−O distances at ~2.00−2.07 Å and one longer Ta2−O1 equatorial distance at ~2.40 Å. The distances and structural connectivity for the tantalum oxide substructure is consistent with previous structural characterization for $Na_2Ta_4O_{11}$.[16]

Within the layer of TaO_6 octahedra, as shown in Figure 4, the Na^+ cations partially occupy an irregular seven-coordinate site (Wyckoff site 12*c*) at Na−O distances of ~2.40 to 2.82 Å, the same as found in fully occupied sites in $Na_2Ta_4O_{11}$. However, the replacement of Na^+ in the structure for Cu^+ is found to occur at a linearly coordinated site (Wyckoff site 18*d*), with two

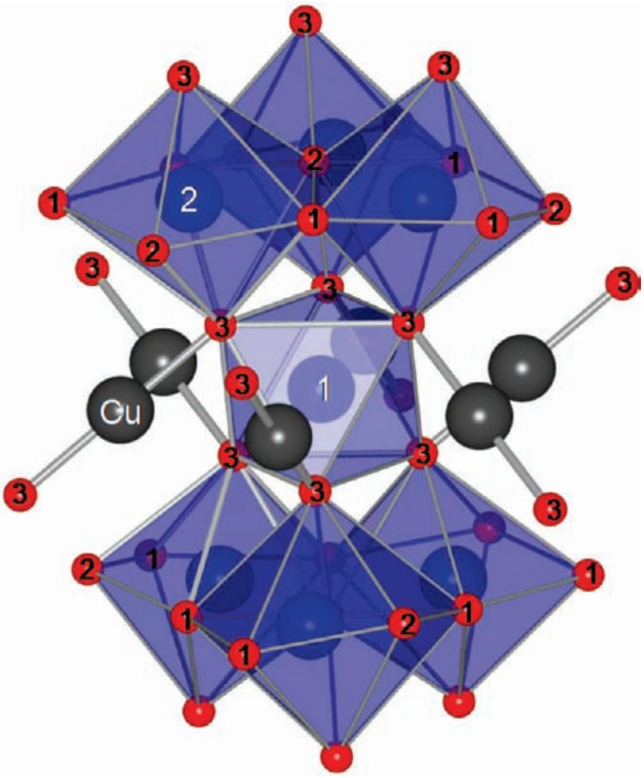

Figure 5. Polyhedral view of the local coordination environments in $(Na_{1-x}Cu_x)_2Ta_4O_{11}$for a single TaO_6 octahedron with three edge-sharing pentagonal bipyramids above and below, and all possible near-neighbor Cu positions. Atom types are numbered for O (red) and Ta (blue polyhedra).

equivalent Cu−O3 distances of ~1.76−1.81 Å in each of the structures. The Cu sites, shown in Figures 4d and 5, reach ~52% site occupancy at the Cu-richest composition of $Na_{0.44}Cu_{1.56}Ta_4O_{11}$. The occupation of near-neighbor Cu sites would yield a closest-attainable Cu−Cu distance of ~3.1 Å, and which is satisfactorily larger than that for previously reported d^{10}-d^{10} Cu^+ near-neighbor distances of down to ~2.53 Å.[24] Also, the Cu site in the structurally-related layers of $Cu_3Ta_7O_{19}$ shows full occupancy can be possible. The combined Na^+/Cu^+ site occupancy, shown together in Figure 4c, decreases from ~88%, to ~81%, to ~74% across the compositions from the Cu-poorest to Cu-richest compositions. The "$Cu_2Ta_4O_{11}$" composition, if reached, would exhibit the lowest combined site-occupancy of ~67%, and which is limited by the charge-balancing requirements. By comparison, the similar $Cu_5Ta_{11}O_{30}$ structure exhibits a Cu-site occupancy of ~83%. Thus, these results indicate that a primary determinant of the stability limit for the $A_xTa_{3n+1}O_{8n+3}$ family is the combined total occupancy of the interlayer A sites, which in this case needs to be at least ~74%. The occupation of near-neighbor Na and Cu sites would yield a closest possible interatomic spacing of ~1.80 Å. Considering that a single Cu site replaces a single Na site, this close contact must occur to some extent randomly within the structure of the solid-solution. However, the strongly preferred coordination environments for Na^+/Cu^+ in this case yield a rare site-differentiated solid-solution.

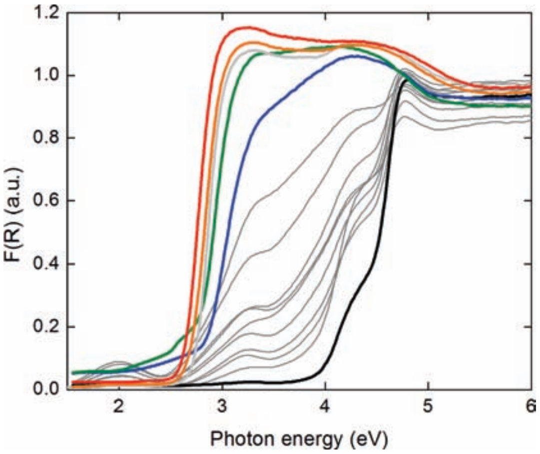

Figure 6. Measured UV−Vis diffuse reflectance spectra for $(Na_{1-x}Cu_x)_2Ta_4O_{11}$ for $x = 0$ (black), 0.01−0.09 (0.01 increments; thin black lines), 0.1 (blue), 0.3 (green), 0.5 (gray), 0.7 (orange), and 0.9 (nominally; red).

As shown in Figure 2, the lattice constants follow a linear relationship with increasing Cu content across the $(Na_{1-x}Cu_x)_2Ta_4O_{11}$ solid solution, with no detectable deviations from Vegard's law. The *a* lattice parameter increases only slightly, at ~0.01 Å, compared to significant increases in the *c* lattice parameter of ~0.3 Å. This is a surprising trend given the significantly smaller Shannon crystal radii of Cu^+ (r = 0.60 Å) compared to Na^+ (r = 1.26 Å) for their respective coordination environments.[25] Consistent with these radii, the height of the layer of Cu^+ cations and isolated TaO_6 octahedra decreases from ~2.139 Å for $x = 0.37$, to ~1.978 Å for $x = 0.78$. This is reflected in the shortening of the Cu−O3 and intra-octahedral Ta1−O3 distances with increasing x, listed in Table 3. However, these decreases are more than offset by the increasing height of the TaO_7 pentagonal bipyramidal layer, which increases from ~3.980 Å for $x = 0.37$ to ~4.165 Å for $x = 0.78$. As shown in Figure 5, these two opposing trends are coupled to each other via the bridging Ta2−O3−Cu interactions between the layers. While the Cu−O3 distances are strengthened and shortened with increasing Cu content, the analogous Ta−O3 distances become weakened and elongated. Further, the increasing Ta2−O3 distances are aligned directly down the *c*-axis and thus predominant over changes in the Cu−O3 distances that have a much more significant in-plane *ab* component.

Optical Properties and Electronic Structures. Bandgap strategies have emerged for extending the range of light absorption in early transition-metal oxides out to the visible-light wavelengths via the incorporation of a late transition-metal or main group elements, for example, Ag^+ or Pb^{2+}.[7,8] This results in a new higher-energy valence band typically composed of the d^{10} or $d^{10}s^2$ electron configuration of the latter. The $(Na_{1-x}Cu_x)_2Ta_4O_{11}$ solid solution enables the first measurements of the changes in bandgap sizes as a function of increasing Cu content, as characterized by the UV−Vis diffuse reflectance data plotted in Figure 6 for $x = 0$−0.1 (in 0.01 increments), 0.3, 0.5, 0.7, and 0.9 (nominally).

---

(24) Lin, H.; Maggard, P. A. *Inorg. Chem.* **2007**, *46*, 1283–1290.

(25) Shannon, R. D. *Acta Crystallogr.* **1976**, *A32*, 751–767.

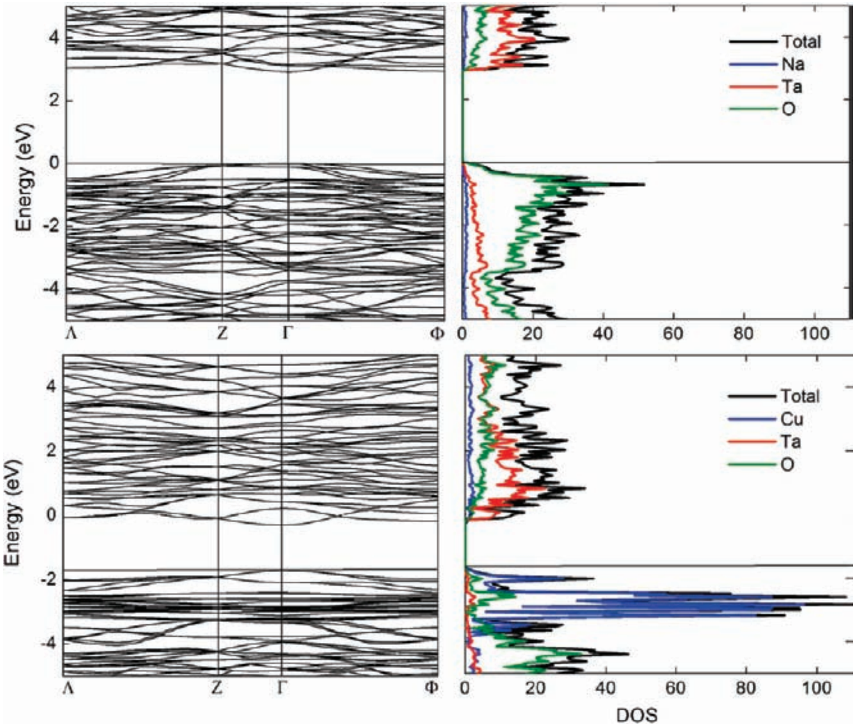

Figure 7. Results of the TB-LMTO-ASA electronic structure calculations for $Na_2Ta_4O_{11}$ (upper) and the "$Cu_2Ta_4O_{11}$" HREM structural model (lower),[12] including the band-structure diagrams (left) and the total and partial densities-of-states for each element (right). The Fermi level is labeled by the solid horizontal lines in each plot.

A substantial red-shift of the optical bandgap size from ~4.0 to = 2.65 eV is found upon going from $x = 0$ ($Na_2Ta_4O_{11}$) to $x = 0.78$ ($(Na_{0.22(3)}Cu_{0.78})_2Ta_4O_{11}$). Notably, at the low Cu^+ content of $x = 0.01-0.05$, a pre-edge peak appears at ~3.2 eV, and which corresponds to the transitions from isolated Cu $3d^{10}$ orbitals prior to their formation of the new valence band. At increasing Cu concentrations, this peak rises rapidly and then broadens slowly to yield the visible-light band edge at ~2.65 eV. Thus, the new Cu $3d^{10}$ valence band is determined to be centered at around ~0.8 eV higher (for $x = 0.05$) than the O 2p valence band of $Na_2Ta_4O_{11}$, and which then further broadens by ~1.1 eV (for $x = 0.78$).

Electronic structures of the two limiting members, $Na_2Ta_4O_{11}$ and "$Cu_2Ta_4O_{11}$", were calculated to determine the atomic and structural origins of the valence and conduction band energies as a function of increasing Cu content. The total and projected Densities of States (DOS) and corresponding band structures were calculated for both, and are shown in Figure 7. In each case, the lowest-energy bandgap excitation is predicted to be direct and located at the Γ point of k-space. The bandgap sizes are calculated to be lower than that obtained experimentally, as is usually found.[26,27] The highest-occupied crystal orbital in $Na_2Ta_4O_{11}$ consists almost exclusively of O 2p-orbitals from the TaO_7 pentagonal bipyramids, whereas the lowest-unoccupied crystal orbital derives from the in-plane Ta 5d orbitals of the TaO_7 pentagonal bipyramids. The substitution of Cu^+ into the structure, that is, in "$Cu_2Ta_4O_{11}$", results in new highest-occupied crystal orbitals that correspond to the filled Cu $3d_{z^2}$ that also mix to a small extent with the O 2p-orbitals. Further, the lowest-unoccupied band components are now composed of the Ta 5d orbitals located on the TaO_6 octahedra rather than on the TaO_7 pentagonal bipyramids. As described earlier, the Cu−O3 interactions weaken the bonding within the pentagonal bipyramids. The lowest-energy bandgap excitations of $Cu_2Ta_4O_{11}$ can therefore be viewed as yielding a metal-to-metal charge transfer transition between the linearly coordinated Cu^+ and the TaO_6 octahedra. Also, these results predict that a higher occupancy at the Cu site would lead to a partial filling of Ta d-orbitals and metallic behavior.

A key question for the Cu(I)-tantalates is whether the band energies resulting from the Cu $3d^{10}$ and Ta $5d^0$ orbitals meet the thermodynamic requirements for driving the water splitting reactions at their surfaces using visible light. A failure to observe these photochemical reactions directly would prove inconclusive, as optimized surface modifications would be necessary to lower the kinetic barriers. Fortunately, the band energies for early transition-metal oxides are known to fairly accurately follow the Butler and Ginley equation based on the geometric mean of the Mulliken electronegativities,[28] as well as the more empirically derived Scaife equation ($V_{fb} = 2.94 - E_g$; V_{fb} = flat-band potential in V; E_g = bandgap size in eV).[29] However, both methods are typically known to fail in the case of metal oxides composed of two or more transition metals. A convenient solution is provided by using the $(Na_{1-x}Cu_x)_2Ta_4O_{11}$ solid solution compositions.

---

(26) Carrasco, J.; Illas, F.; Lopez, N.; Kotomin, E. A.; Zhukovskii, Y. F.; Evarestov, R. A.; Masrikov, Y. A.; Piskunov, S.; Maier, J. *Phys. Rev. B* **2006**, *73*, 064106–064111.

(27) Piskunov, S.; Heifets, E.; Eglitis, R. I.; Borstel, B. *Comput. Mater. Sci.* **2004**, *29*(2), 165–178.

(28) Butler, M. A.; Ginley, D. S. *J. Electrochem. Soc.* **1978**, *125*, 228–232.

(29) Scaife, D. E. *Solar Energy* **1980**, *25*, 41–54.

Application of the Scaife equation to $Na_2Ta_4O_{11}$ locates the O 2p valence band at +3.0 V and the Ta d^0 band at −1.0 V versus the standard hydrogen electrode, as found for $Na_2Ta_4O_{11}$ and $NaTaO_3$. From the UV−Vis DRS spectra, the Cu $3d^{10}$ orbitals are shown to initially emerge at ~0.8 eV higher than the O 2p valence band, that is, at +2.2 V on the redox scale. At the highest Cu content of $x = 0.78$, the $3d^{10}$ band has broadened and reduced the bandgap size by another 0.55 eV, that is, or up to +1.65 V on the redox scale. Thus, the resultant conduction and valence band energies are suitably positioned (i.e., above and below, respectively) the reduction and oxidation potentials for water splitting, which are located at 0.0 V (H_2O/H_2) and +1.23 V (O_2/H_2O) under standard conditions. More generally, these results demonstrate a promising new approach in the utilization of cation substitutions, amenable to a number of metal oxides, to probe the formation and position of the higher-energy valence bands required for new photocatalytic metal oxides.

Conclusions

The new $(Na_{1-x}Cu_x)_2Ta_4O_{11}$ ($0 \leq x \leq 0.78$) solid-solution can be prepared via standard solid-state reactions in evacuated fused-silica vessels. The tantalate substructure consists of single layers of pentagonal TaO_7 bipyramids as well as layers of isolated TaO_6 octahedra. The site-differentiated occupation of separate Na and Cu positions results from their disparate preferences in coordination geometries, either seven-coordinate for the former or a linear coordination geometry for the latter. Their combined occupancy decreases with x, but ultimately reaches a lower limit of stability at ~74% for $x = 0.78$. This provides a new insight into the stability or lack thereof in related members of the $Cu_xTa_{3n+1}O_{8n+3}$ family. A significant red-shift of the bandgap size from ~4.0 to ~2.65 eV is found with increasing Cu content, and which arises from the creation of a new higher-energy valence band resulting from the incorporation of the $3d^{10}$ orbitals within $Na_2Ta_4O_{11}$. Diffuse reflectance measurements at both low and high Cu content enables the characterization of the formation of the new higher-energy valence band. These result show that both the conduction and the valence band energies favorably bracket the redox potentials for water reduction and oxidation, and thus provide a promising new family of solids to investigate for the solar-driven photocatalysis of water.

Acknowledgment. The authors acknowledge support of this research from the Chemical Sciences, Geosciences and Biosciences Division, Office of Basic Energy Sciences, Office of Science, U.S. Department of Energy (DE-FG02-07ER15914), and also assistance with the collection of high-resolution PXRD data (H.-C. zur Loye).

Supporting Information Available: A table including the full details of the three powder X-ray structural refinements. This material is available free of charge via the Internet at http://pubs.acs.org.